

Quantitative Analysis of High Frequency Material Properties in Thin-Ribbon Magnetic Cores

Marcin Szewczyk¹, Senior Member, IEEE, Kamil Kutorasiński², Wojciech Piasecki¹, Member, IEEE

¹ABB Corporate Research Center, Kraków, Poland

²AGH University of Science and Technology, Kraków, Poland

This paper presents quantitative analysis of material properties of magnetic cores wound of thin magnetic tape. Self-consistent model of penetration depth was proposed to include skin effect in calculation of magnetic material parameters. The model was used to extract geometry-independent material parameters based on which quantitative analysis of the material complex permeability was presented. The model is based on the magnetic cores frequency dependent complex impedance (measured) and on selected basic material parameters (typically provided by manufactures). The approach is demonstrated on a practical example in which frequency dependent saturation current of the magnetic cores was calculated based on the extracted geometry-independent material parameters. The results are presented for three types of nanocrystalline cores, in a frequency range from 1 kHz to 100 MHz.

Index Terms—Magnetic cores, magnetic ribbon, magnetic properties, permeability model, skin effect, saturation current.

I. INTRODUCTION

IN NANOCRYSTALLINE and amorphous thin tape-based soft magnetic materials eddy current losses are reduced as compared to standard FeSi-sheets because of small thickness of the material thin-film ribbons [1]. The nanocrystalline ribbons are typically around 20 μm thick, as achieved by rapid solidification from melt [2], [3]. For this thickness, the skin effect impact on the magnetic core parameters (such as permeability) is smaller than in the standard FeSi sheets, however, becomes more significant than it is for powder materials, specifically in higher frequency range [4]. Among other superior soft magnetic properties, the material also reveals high relative permeability, high saturation induction, and good high frequency behavior. These properties causes that thin-ribbon cores are being increasingly used in various applications, from low-power electronic devices [8], up to high power components [9].

For given material types, it is often required by magnetic designers and application engineers to identify material-specific characteristics in order to study the material behavior over wide frequency range [5]. Typically, only basic material properties are provided by manufactures, while other parameters have to be measured and extracted by the magnetic designers themselves.

For high frequency applications the specific core characteristics are needed to be known over a wide frequency range. The state-of-the art methods provide the magnetic core characteristics for the specific geometry of the core [10]. This paper presents a method of obtaining geometry-independent material parameters. The method is based on the measured frequency characteristics of a magnetic core complex impedance Z^* and on the core material physical parameters (such as core geometry, ribbon thickness, ribbon resistivity, etc.). The measurement of the complex impedance Z^* over a given frequency range can be performed using a network

analyzer. The basic material parameters as used in this paper are typically provided by material manufacturers in the material data-sheets (e.g. [3]).

Self-consistent model of penetration depth was presented to include the skin effect in the calculation of the magnetic core effective cross-section area A_e . The model was then used to extract geometry-independent material parameters and to present quantitative analysis of the skin effect impact on the material properties, such as magnetic complex permeability.

The model presented was then applied to calculate frequency dependent saturation current of magnetic cores. These results can be specifically applicable for magnetic cores used for mitigating of high frequency transients in high power applications [9], [11]. In this case, typically a simplified modeling approach is used, either based on a linear inductive element model with a fixed inductance value, or based on a simple frequency independent inductor model with the saturation characteristics included. These simplified models were used e.g. in [11].

The method and the results described in the present paper are demonstrated using practical examples of three types of commercially available nanocrystalline cores, over a frequency range from 1 kHz to 100 MHz.

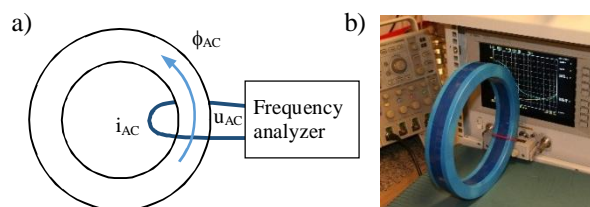


Fig. 1. Measurement set-up of complex impedance frequency characteristics $Z^*(f)$: (a) schematic diagram, (b) physical arrangement.

II. MAGNETIC CORE MATERIAL CHARACTERIZATION

The study reported in this paper was conducted for three types of nanocrystalline cores characterized by the same geometry and different material properties. The cores are

Manuscript received October 1, 2014. Corresponding author: M. Szewczyk (e-mail: marcin.szewczyk@pl.abb.com).

Color versions of one or more of the figures in this paper are available online at <http://ieeexplore.ieee.org>

denoted as [3]: Core 1, Core 2, and Core 3. The following subsections of the paper present material characterization of the cores on the basis of the measured frequency characteristics of complex impedance Z^* and on basic material parameters (typically provided by manufacturer).

A. Frequency characteristics of complex impedance

Measurements of complex impedance Z^* were performed with the use of an impedance analyzer (Agilent 4294A). For each core type, the measurements were conducted for a set of 4 cores (12 cores in total) to check parameters variations for the cores of a given type. Characteristics were measured over a frequency f range from 1 kHz to 100 MHz.

Schematic diagram and physical arrangement of the measurement set-up are shown in Fig. 1. Fig. 2 shows frequency dependent complex impedance $Z^*(f)$ measured for one selected core of each type:

$$Z^*(f) = |Z^*(f)|e^{j\varphi(f)}, \quad (1)$$

where: $|Z^*(f)|$ is amplitude, and $\varphi(f)$ is phase angle of the complex impedance $Z^*(f)$. Characteristics for different cores of a given type revealed relatively small variation of $|Z^*(f)|$ and $\varphi(f)$ (less than 5%), excluding one core of type 3 (where difference of more than 10% from average value was observed in a low frequency range from 1 kHz to 10 kHz) and one core of type 2 (where difference exceeding 15% was observed in a frequency range from 1 MHz to 100 MHz).

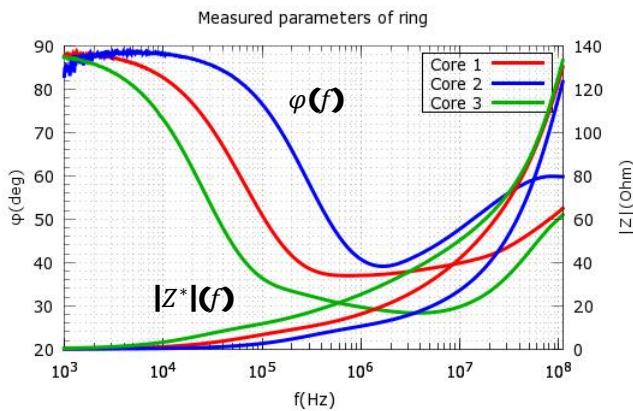


Fig. 2. Measurement results of complex impedance $Z^*(f)$: amplitude $|Z^*|$ and phase angle φ ; for three types of nanocrystalline cores, as used in calculations.

From Fig. 2 it can be seen that in the low frequency range the cores of all types have the impedance phase angle of $\varphi \approx 90$ deg and the impedance amplitude $|Z^*|$ is close to zero, therefore they behave like lossless small inductances. In high frequency range $|Z^*|$ increases and the phase angle φ differs from 90 deg, thus they act like highly lossy inductors.

B. Additional basic material properties

Calculations presented in this paper require only few basic material parameters in addition to the measured complex impedance $Z^*(f)$ as presented above (see Fig. 2). These material properties were used as available in the manufacturer

data-sheets [2] (exemplary values are given in brackets): ribbon conductivity ($\sim 100 \mu\Omega\cdot\text{cm}$), ribbon thickness ($\sim 20 \mu\text{m}$), saturation flux density B_{sat} (1.2 T), core geometry: specified by effective cross-section area of the core A_e ($\sim 400 \text{ mm}^2$) and effective magnetic path length l_e ($\sim 0.6 \text{ m}$), packaging factor of ribbons (allowing to calculate geometrical cross-section area A_g of the ribbons based on the core dimensions; ~ 0.75), relative permeability μ_r (given for frequency 10 kHz and having different value for each of the core type; Core 1: 8000, Core 2: 30000, Core 3: 80000).

III. CALCULATION OF INDUCTANCE WITH MAGNETIC LOSSES

A. Equivalent circuit of complex impedance

Equivalent circuit diagrams give an intuitive description of complex quantities such as the complex impedance of the magnetic cores Z^* . To extract physical and therefore more intuitive parameters from the measured $|Z^*|$ and φ , series resistance R_s and series inductance L_s of the impedance $Z^* = R_s + j\omega L_s$ were calculated at given frequency $f = \omega/2\pi$ (see inset in Fig. 3 for equivalent circuit diagram):

$$\begin{aligned} R_s(f) &= \text{Re}(Z^*) = |Z^*| \cos(\varphi) \\ L_s(f) &= \text{Im}(Z^*)\omega^{-1} = |Z^*| \sin(\varphi)\omega^{-1} \end{aligned} \quad (2)$$

Results of the calculated $R_s(f)$ and $L_s(f)$ characteristics are shown in Fig. 3. It can be noticed that in the low frequency range all cores behave like lossless inductances (with negligible R_s as compared to $j\omega L_s$) and above some frequency value (different for each of the core type) they start to lose inductive properties in a favor of the resistive behavior (see also Fig. 2). Initial low frequency values of the inductances are also indicated in Fig. 3.

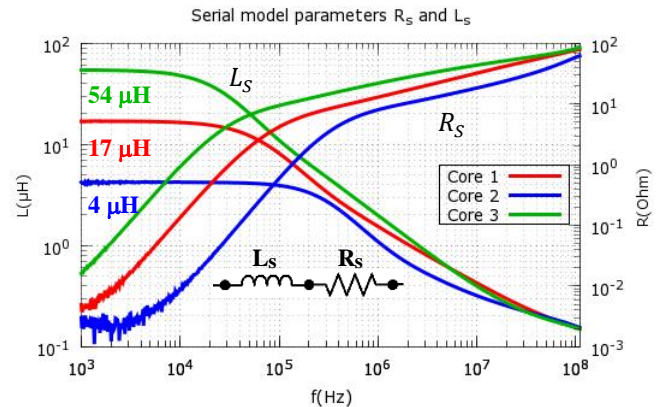


Fig. 3. Series equivalent model $L_s(f)$ and $R_s(f)$ of impedance $Z^*(f)$, as per (2).

B. Complex permeability

Complex behavior of magnetic core impedance implies magnetic losses in the core material. Magnetic losses can be also modeled by introducing the complex frequency-dependent relative permeability $\mu_r^*(f) = \mu'(f) - j\mu''(f)$, whose imaginary part μ'' accounts for hysteresis losses [4]. This implies that the complex impedance Z^* for 1-turn coil becomes a function of a complex inductance L^* [4]:

$$\begin{aligned} Z^* &= j\omega L^* = j\omega\mu_0\mu_r^* \frac{A_e}{l_e} = j\omega\mu_0(\mu' - j\mu'') \frac{A_e}{l_e} \\ &= j\omega \frac{\mu_0\mu' A_e}{l_e} + \omega \frac{\mu_0\mu'' A_e}{l_e} \end{aligned} \quad (3)$$

Then, the permeability μ_r^* can be expressed directly by $|Z|$, φ :

$$\begin{aligned} \mu'(f) &= \text{Im}(Z^*) \frac{l_e}{\omega\mu_0 A_e} = \frac{|Z^*| \sin(\varphi) l_e}{\omega\mu_0 A_e}, \\ \mu''(f) &= \text{Re}(Z^*) \frac{l_e}{\mu_0 A_e} = \frac{|Z^*| \cos(\varphi) l_e}{\mu_0 A_e}. \end{aligned} \quad (4)$$

The results of calculated $\mu'(f)$ and $\mu''(f)$ are shown in Fig. 4, where frequencies (f_1, f_2, f_3) are indicated for which the imaginary part μ'' starts to have significant contribution to the permeability absolute value $|\mu_r^*| = \sqrt{\mu'^2 + \mu''^2}$ (μ''^2 becomes more than 5% of μ'^2). The low frequency permeability values are in agreement with the data provided by manufacturer.

Both approaches of magnetic losses description (through series equivalent circuit diagram and complex permeability) can be combined, such as R_s and L_s can be expressed through μ'' and μ' respectively:

$$R_s(f) = \omega \frac{\mu_0\mu'' A_e}{l_e}, \quad L_s(f) = \frac{\mu_0\mu' A_e}{l_e}. \quad (5)$$

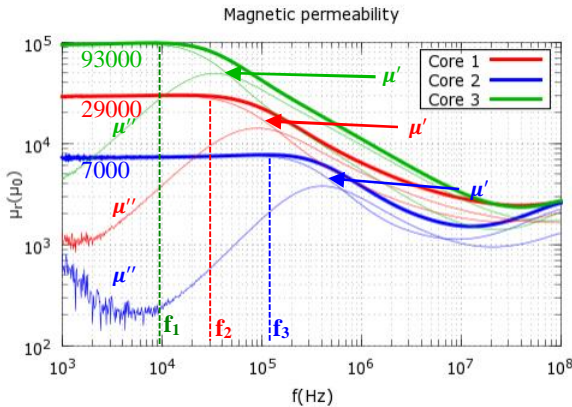


Fig. 4. Complex magnetic permeability according to (4). Thick lines: absolute value of permeability $|\mu|$, thin lines: real μ' and imaginary parts μ'' . Frequencies f_1, f_2, f_3 indicate noticeable impact of μ'' . Numbers indicate low frequency permeability limits.

C. Skin effect

Parameters $\mu'(f)$ and $\mu''(f)$ depend on the magnetic core effective cross-section area A_e , which can be significantly different from the core geometrical cross-section area A_g , specifically in the high frequency range. Since hysteresis losses are relatively small in nanocrystalline materials [2], the eddy currents (and the corresponding skin effect) play major role in energy dissipation processes. To include this effect, penetration depth $\delta(f)$ was analyzed:

$$\delta(f) = \sqrt{\frac{2}{\omega\sigma\mu_0\mu_r(f)}}, \quad (6)$$

where $\mu_r(f)$ is the frequency dependent relative permeability, μ_0 is permeability of vacuum, σ is electrical conductivity [S/m], and $\omega = 2\pi f$ is angular frequency. The conductivity was assumed constant within the specified frequency range [6].

Fig. 5 shows the calculated skin effect, where the frequencies (f_1, f_2, f_3) are indicated, at which the skin depth is equal to the ribbons thickness ($20 \mu\text{m}$). They have the same values as the frequencies for which the imaginary part of permeability (and therefore the eddy current losses) start to have significant contribution to the permeability absolute value (see Fig. 4).

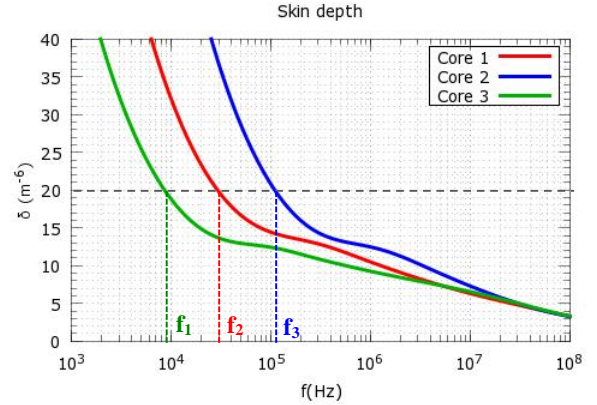


Fig. 5. Skin depth according to (6), calculated with the use of material frequency dependent permeability. Horizontal dashed line marks ribbon thickness. Frequencies f_1, f_2, f_3 indicate value where skin depth is equal to the ribbon thickness.

IV. MAGNETIC CORE EFFECTIVE CROSS-SECTION AREA

A. Skin effect impact on effective cross section area

In the formula describing frequency dependent permeability, as given by (4), the bulk material properties can be separated from the geometrical effects. It is shown in Fig. 5 that in the high frequency range, for which the skin depth is below 1/4 of the ribbon thickness ($20 \mu\text{m}$), only a small fraction of the ribbon is penetrated by the magnetic field. The cross section area of the magnetic core can thus be treated not as a constant geometric value A_g but as a frequency dependent effective cross section area $A_e(f)$ (indicating the actual use of the material). As in the high frequency range $A_e(f)$ is much lower than A_g , by not taking into account the skin effect (6) in (4) the permeability would be underestimated in the high frequency range.

By taking into consideration the skin effect in the material equations (4), one can extract bulk material frequency independent parameters.

B. Model of magnetic core effective cross-section area

To extract geometry independent material parameters, a formula for the magnetic core effective cross-section area $A_e(f)$ is proposed:

$$A_e(f) = w(f)A_g, \quad (7)$$

where $w(f)$ is a weight function here introduced to represent the penetration depth of the magnetic field into the material, and A_g is the material geometrical cross-section area.

The magnetic flux density B in a conductive material

decreases exponentially at any given depth x from the surface, starting from its value at the surface B_0 , according to the formula:

$$|B(x)| = |B_0|e^{-x/\delta}, \quad (8)$$

where $\delta = \delta(f)$ is the frequency dependent skin depth, as given by (6). By combining (7) and (8), the weight function $w(f)$ can be calculated for a ribbon thickness d (for rectangular cross-section):

$$w(f) = \frac{A_e(f)}{A_g} = \frac{B_0 A_e(f)}{B_0 A_g} = \frac{\phi_e(f)}{\phi_g} = \frac{h \int_0^d B(x) dx}{h B_0 d}, \quad (9)$$

where the $\phi_e(f)$ and ϕ_g are magnetic fluxes through A_e and A_g cross-section areas respectively, and h is the ribbon width.

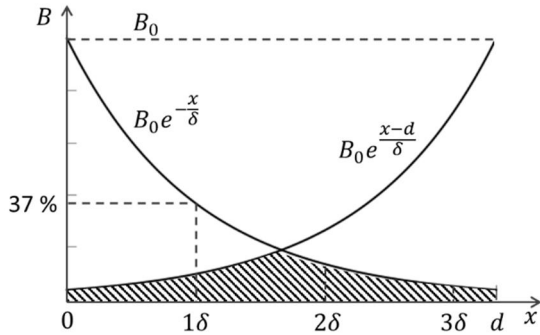


Fig 6. Schematic picture of penetration depth. Magnetic field penetrates material with thickness d from both sides. Overlapping area is marked, which has to be subtracted in calculation of weight function, see (11).

Assuming that the ribbon is penetrated from its both sides:

$$B(x) = |B_0|e^{-x/\delta} + |B_0|e^{-x-d/\delta}, \quad (10)$$

and keeping in mind that the area where the field from both sides overlaps should be counted only once (see Fig. 6), the weight function $w(f)$ can be expressed as:

$$w(f) = \frac{1}{d} \int_0^d e^{-x/\delta} + e^{-x-d/\delta} - e^{-x/\delta} e^{-x-d/\delta} dx \quad (11)$$

$$= \frac{2\delta}{d} \left(1 - e^{-d/\delta}\right) - e^{-d/\delta}.$$

The frequency dependency of $w(f)$ is thus determined by the frequency dependency of the skin depth $\delta(f)$.

V. QUANTITATIVE ANALYSIS OF SKIN EFFECT IMPACT ON MAGNETIC PERMEABILITY

A. Method of calculation

After knowing the weight function $w(f)$, as given by (11), and therefore the effective cross section area $A_e(f)$ of the core, the geometry independent material permeability μ^* can be calculated:

$$\mu' = \frac{|Z^*| \sin(\varphi) l_e}{\omega \mu_0 w(f) A_g}$$

$$\mu'' = \frac{|Z^*| \cos(\varphi) l_e}{\mu_0 w(f) A_g} \quad (12)$$

where $w(f)A_g$ substitutes for A_e in (4).

The magnetic permeability μ^* depends on the cross section area $A_e = w(f)A_g$, which depends on the penetration depth δ , which in turn depends on μ^* . This makes the problem of solving (12) entangled and force to use a self-consistent method. The scheme of the method is shown in Fig. 7. To extract μ' , μ'' , A_e , and δ from $|Z^*|$ and φ , the initial value of magnetic permeability μ_r^{init} was used to start the iterative process of calculation. In practice, μ_r^{init} should be selected within reasonable limits (e.g. between 1000 and 100 000).

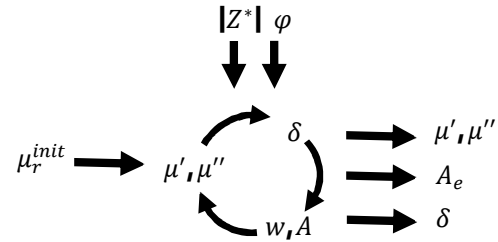


Fig 7. Diagram of self-consistent method for calculation of frequency dependent material parameters. Measured $|Z^*|$ and φ are used as inputs and μ' , μ'' , A_e , and δ are the results. μ_r^{init} is used to start the iterative process.

B. Calculation results

The self-consistent method described above was applied to calculate the magnetic permeability of the three selected and previously described nanocrystalline cores. The solution obtained according to Fig. 7 reached convergence after less than 10 iterations. For initial magnetic permeability μ_r^{init} the values calculated for 10 kHz (see Fig 4) were used.

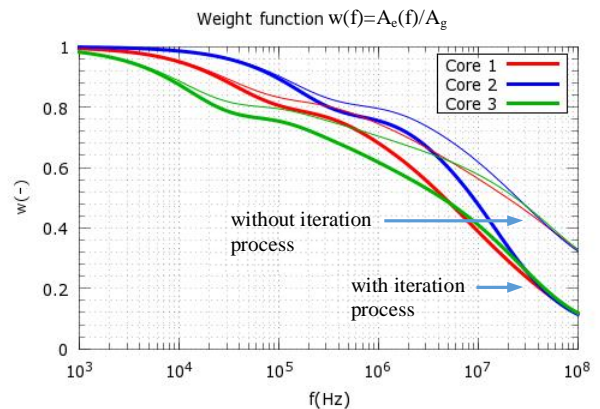


Fig 8. Weight function $w(f)$ according to (11), showing actual usage of material. Thick and thin line show $w(f)$ after convergence and in first iteration respectively.

Fig. 8 and Fig. 9 show the weigh function $w(f)$ and the skin depth respectively, calculated in the frequency range from 1 kHz to 100 MHz. Fig. 10 shows the real part μ' of the complex magnetic permeability μ^* according to (12). Thick and

thin lines in Fig. 8-10 show the corresponding qualities with and without the iteration process respectively.

The values of the weight function $w(f)$ (see Fig. 8) in the low frequency range (i.e. approx. below 1 kHz) approximately equal to unity, which shows that below 1 kHz the magnetic field penetrates the entire material of the core (i.e. $A_e(f) = A_g$). In the high frequency range (up to 100 MHz) the skin depth δ (see Fig. 9) is approx. few μm (below the ribbon thickness) and therefore the weight function (see Fig. 8) is significantly lower (approx. 15%) than the low frequency value.

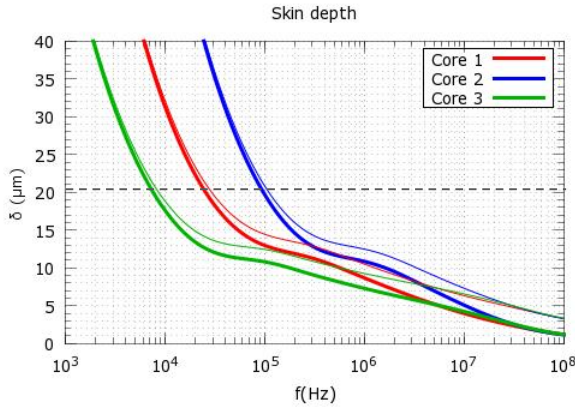


Fig. 9. Magnetic skin depth δ calculated according to (6). Thick and thin lines show $\delta(f)$ after convergence and in first iteration respectively. Horizontal dashed line marks average ribbon thickness.

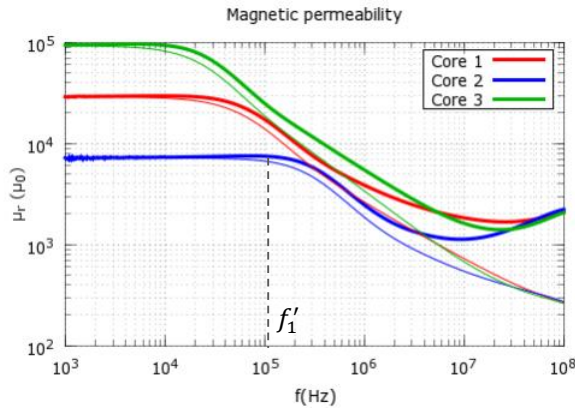


Fig. 10. Real permeability $\mu'(f)$, according to (12) (pure material). Thick and thin lines show $\mu'(f)$ after convergence and in first iteration respectively. Dashed vertical line marks first resonance frequency in Table I.

The significant change in the weight function $w(f)$, as well as in the penetration depth δ , with the iterative procedure was also observed. The iteration impact increases with the increase in the frequency (see thick and thin lines in Fig. 8 and Fig. 9). It concludes that without the iterative procedure, $w(f)$ and $\delta(f)$ (and therefore $A_e(f)$) are underestimated for high frequencies. This follows that at high frequencies the magnetic permeability is much underestimated without the iteration procedure (even 10 times at 100 MHz, see Fig. 10).

VI. CALCULATION OF SATURATION CURRENT

Magnetic cores are often modeled by frequency dependent complex linear impedance, exemplarily expressed by the series impedance $Z^*(f) = R_s + j\omega L_s$ [7]. The impedance can be then

modeled as a lumped element equivalent circuit, which can be further directly implemented in a circuit simulation software (such as e.g. EMTP, Matlab/Simulink, or PSCAD) for low- or high-power simulations. As the magnetic cores are non-linear elements (due to their non-linear magnetization $B(H)$ characteristics), in many applications it is important to determine the saturation current value I_{sat} above which the core reveals its non-linear behavior. This is specifically of concern for when the magnetic cores are applied for mitigating of high frequency transients in high power applications [9, 11].

The saturation current I_{sat} can be resolved using Ampère's law, i.e. curl of $H = B/(\mu_0\mu_r)$ over effective magnetic path length l_e : $\oint H dl = I$, from which: $H_{sat}l_e = I_{sat}$. Full formula for I_{sat} can be then derived as:

$$I_{sat}(f) = \frac{B_{sat}l_e}{\mu_0\mu_r(f)} = \frac{B_{sat}l_e}{\mu_0} \frac{\mu_0 A(f)}{L_s(f)l_e} = \frac{B_{sat}A(f)}{L_s(f)} = \frac{B_{sat}A_g w(f)}{L_s(f)} = \frac{2\pi f B_{sat} A_g w(f)}{|Z(f)| \sin \varphi(f)} \quad (13)$$

where all of the qualities are defined in the preceding sections.

The results of calculated I_{sat} are shown in Fig. 11. The weight function $w(f)$ in (13) was calculated iteratively with the approach presented previously, so that the saturation current I_{sat} was changing with the iteration number n (again, thick and thin lines in Fig. 11 show the results with and without the iterations process respectively). Inset in Fig. 11 shows the I_{sat} values for low frequencies, starting from 1 kHz.

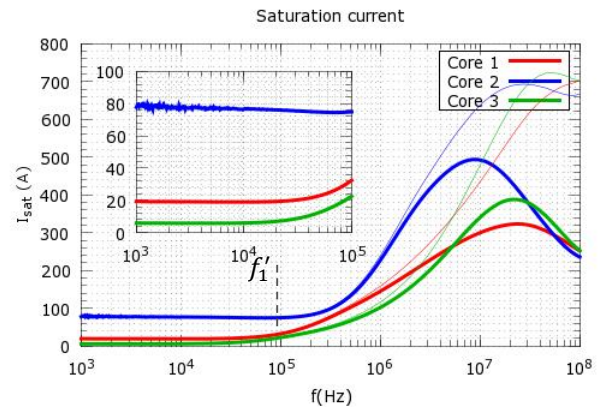


Fig. 11. Saturation current I_{sat} according to (13) (limit of linearity of core equivalent circuit model). Thick and thin lines show I_{sat} after convergence and in first iteration respectively.

It can be noticed that below 100 kHz, the saturation current I_{sat} is almost constant with frequency. Above 100 kHz it increases rapidly, which is related to the decrease of $\mu_r(f)$ (see e.g. f'_1 in Fig. 10 and Fig. 11). Above frequency 10 MHz, where the high frequency effects start to play a role (see Fig. 11), the saturation current I_{sat} increases. Comparison of thick and thin lines in Fig. 11 indicates that by not including the iteration procedure (see Fig. 7) the saturation current I_{sat} would be overestimated in the high frequency range.

It can also be concluded that by not taking into account the skin effect in (13), the saturation current I_{sat} would be overestimated in high frequency range by factor $w(f)$ (e.g. approx. 10 times for 100 MHz according to Fig. 8).

VII. CONCLUSIONS

Nanocrystalline and amorphous alloys are widely used for soft magnetic applications in a form of thin ribbons, typically around 20 μm thick. For that thickness value the skin effect has a reduced impact on magnetic core parameters (such as permeability), however with increasing importance in high frequency range.

In this paper a quantitative evaluation of material properties was presented for three types of commercially available nanocrystalline cores, in a frequency range from 1 kHz to 100 MHz. Based on the measured complex impedance and typically available basic material parameters, the skin effect impact on the material properties was modeled. The results indicated the importance of the skin effect in medium range of frequency ($10^4 - 10^6$ Hz). Iterative procedure of self-consistent model was employed to calculate the material permeability and saturation current of the cores. Weight function in Fig. 8 represents the quantitative impact (in percentage) of the skin-effect on the material permeability. The results indicated that the calculation of the saturation current at 100 MHz is influenced by the skin effect by factor 10 (see Fig. 8). The saturation current frequency characteristics (see Fig. 11) gives the boundary value of the frequency range, in which the magnetic core equivalent circuit model can be considered as linear.

REFERENCES

- [1] S. Flohrera, R. Schäfer, J. McCorda, S. Roth, L. Schultza, and G. Herzer, "Magnetization loss and domain refinement in nanocrystalline tape wound cores," *Acta Materialia*, vol. 54, no. 12, pp. 3253–3259, July 2006
- [2] G. Herzer, *Magnetic Hysteresis in Novel Magnetic Materials*, chapter *Amorphous and Nanocrystalline Soft Magnets*, pp. 711-730, Kluwer Academic Publishers, 1997.
- [3] Magnetec GmbH, "Product specification for inductive components," [Online] (material data sheet). Available: www.magnetec.de, 2014.
- [4] J. C. Mallinson, *The Foundations of Magnetic Recording*, Academic Press, Inc., San Diego, 1987.
- [5] L. Dalessandro, W. G. H. Odendaal, and J. W. Kolar, "HF Characterization and Nonlinear Modeling of a Gapped Toroidal Magnetic Structure," *IEEE Trans. Power Electronics*, vol. 21, issue 5, pp. 1167 – 1175, 2006.
- [6] W. Li, Y. Sun, and C. R. Sullivan, "High-Frequency Resistivity of Soft Magnetic Granular Films," *IEEE Trans. Magn.*, vol. 41, no. 10, pp. 3283-3285.
- [7] P. G. Blanken and J. J. L. M. Van Vlerken, "Modeling of electromagnetic systems," *IEEE Trans. Magn.*, vol. 27, no. 6, pp. 4509–4515, Nov. 1991.
- [8] L. Dalessandro, N. Karrer, and J.W. Kolar, "A novel isolated current sensor for high-performance power electronics applications," *21st IEEE Applied Power Electronics Conference and Exposition, APEC 2006*, pp. 559-566.
- [9] Y. Guan, G. Yue, W. Chen, and Z. Li, W. Liu, "Experimental Research on Suppressing VFTO in GIS by Magnetic Rings," *IEEE Trans. Power Delivery*, vol. 28, No. 4, pp. 2558-2565, Oct 2013.
- [10] X. Chucheng and W.G. Odendaal, "Frequency Scaling Effects of Integrated Passive Components in High Frequency Power Conversion," Conference Record of the 2006 IEEE Industry Applications Conference, 2006, 41st IAS Annual Meeting, vol. 4, pp. 1841-1848, 8-12 Oct. 2006.
- [11] D. Smugala, W. Piasecki, M. Ostrogorska, M. Florkowski, M. Fulczyk, O. Granhaug, "Wind Turbine Transformers Protection Method Against High-Frequency Transients," *IEEE Trans. Power Delivery*, to be published (published at IEEEXplore).



Marcin Szewczyk (M'2012–SM'2014), born in Koszalin, Poland in 2 September 1974, received his M.Sc. and Ph.D. degrees in Electrical Engineering from Warsaw University of Technology, Poland, in 2000 and 2009, respectively. Since February 2010 he has been working as a researcher in ABB Corporate Research in Cracow, Poland, where he has been involved in various technology development projects. His research and professional interests are mainly in the field of power system analyses and advanced simulations, transients analyses and transients mitigation, insulation coordination studies, 3D modelling and simulations of electromagnetic fields, and system concepts. (ABB Corporate Research, Starowisna 13A, 31-038 Krakow, Poland, E-mail: marcin.szewczyk@pl.abb.com). Dr. Szewczyk is a senior member of IEEE and Polish Society for Theoretical and Applied Electrical Engineering.



Kamil Kutorasiński was born in 1985, received his M.Sc. in physics from the University of Science and Technology in Kraków, Poland where, from 2009, is the PhD student. His research are in the field of transport properties calculation in advanced material based on *ab initio* DFT methods as well as FEM modelling and simulations of electromagnetic fields. (Faculty of Physics and Applied Computer Science, AGH University of Science and Technology, Al. A. Mickiewicza 30, 30-059 Krakow, Poland, E-mail: kamil.kutorasinski@fis.agh.edu.pl)



Wojciech Piasecki was born in Poland on May 15, 1966. He received the M.Sc. degree in electronics from the University of Science and Technology, in Kraków Poland, Poland, and the Ph.D. degree from the Jagiellonian University, Kraków. He has been working for many years in electromagnetic and electrical phenomena, including high-frequency and nonlinear modeling of electrical equipment. Currently, he is a Researcher with the Corporate Research Center in Kraków. His main research concentrates around transient network phenomena analysis.